J Membrane Biol (2013) 246:959–966
DOI 10.1007/s00232-013-9599-7

Functional Investigation of Transmembrane Helix 3 in H^+-Translocating Pyrophosphatase

Ching-Hung Lee · Yen-Wei Chen · Yun-Tzu Huang · Yih-Jiuan Pan · Chien-Hsien Lee · Shih-Ming Lin · Lin-Kun Huang · Yueh-Yu Lo · Yu-Fen Huang · Yu-Di Hsu · Shih-Chung Yen · Jenn-Kang Hwang · Rong-Long Pan

Received: 20 June 2013 / Accepted: 24 September 2013 / Published online: 10 October 2013

Abstract H^+-translocating pyrophosphatase (H^+-PPase, EC 3.6.1.1) plays an important role in acidifying vacuoles by transporting protons across membranes at the expense of pyrophosphate (PP_i) hydrolysis. *Vigna radiata* H^+-PPase (*Vr*H^+-PPase) contains 16 transmembrane helices (TMs). The hydrophobicity of TM3 is relatively lower than that of most other TMs, and the amino acids in this TM are highly conserved in plants. Furthermore, TM5 and -6, which are the core TMs involving in H^+-PPase functions, are near TM3. It is thus proposed that TM3 is associated with H^+-PPase activity. To address this possibility, site-directed mutagenesis was applied in this investigation to determine the role of TM3 in *Vr*H^+-PPase. Upon alanine/serine substitution, T138 and S142, whose side chains face toward the center TMs, were found to be involved in efficient proton transport. G149/S153 and G160/A164 pairs at the crucial termini of the two GxxxG-like motifs are indispensable in maintaining enzymatic activities and conformational stability. Moreover, stability in the vicinity surrounding G149 is pivotal for efficient expression. S153, M161 and A164 are critical for the K^+-mediated stimulation of H^+-PPase. Taken together, our results demonstrate that TM3 plays essential roles in PP_i hydrolysis, proton transport, expression, and K^+ stimulation of H^+-PPase.

Keywords Proton-translocating pyrophosphatase · Proton transport · Transmembrane helix · Site-directed mutagenesis · Coupling efficiency · GxxxG-like motif

Introduction

Vacuolar H^+-pyrophosphatase (H^+-PPase, EC 3.6.1.1) primarily exists in plants and some algae, protozoa and prokaryotes (Maeshima 2000; Drozdowicz and Rea 2001; Serrano et al. 2004). By hydrolyzing pyrophosphate (PP_i), H^+-PPase is capable of pumping protons across membranes to build up an electrochemical gradient for transporting substances, such as ions, metabolites and even toxicants, into vacuoles (Maeshima 2000). A line of evidence indicates that H^+-PPase is a homodimer with a molecular mass of approximately 71–80 kDa for each subunit (Maeshima 2000; Liu et al. 2009; Lin et al. 2012). Furthermore, Mg^{2+} combines with PP_i to form a Mg–PP_i complex as a physiological substrate for H^+-PPase (Maeshima 1991; Gordon-Weeks et al. 1996). PP_i hydrolysis could be stimulated by high concentrations of K^+ but is suppressed by Na^+, Ca^{2+} and F^- (Maeshima 2000, 2001). However, several studies have demonstrated the existence of another type (type II) of H^+-PPase that is insensitive to K^+ (Drozdowicz et al. 2000; Drozdowicz and Rea 2001).

Ching-Hung Lee and Yen-Wei Chen contributed equally to this study.

Electronic supplementary material The online version of this article (doi:10.1007/s00232-013-9599-7) contains supplementary material, which is available to authorized users.

C.-H. Lee · Y.-W. Chen · Y.-T. Huang · Y.-J. Pan · C.-H. Lee · S.-M. Lin · L.-K. Huang · Y.-Y. Lo · Y.-F. Huang · Y.-D. Hsu · R.-L. Pan (✉)
Department of Life Science, Institute of Bioinformatics and Structural Biology, College of Life Science, National Tsing Hua University, Hsin Chu 30013, Taiwan, Republic of China
e-mail: rlpan@life.nthu.edu.tw

S.-C. Yen · J.-K. Hwang
Institute of Bioinformatics, National Chiao Tung University, Hsin Chu 30050, Taiwan, Republic of China

Each subunit of H^+-PPase in *Vigna radiata* contains 16 transmembrane helices (TMs) forming two concentric walls as observed from its X-ray crystal structure (Lin et al. 2012). The inner wall is composed of TM5, TM6, TM11, TM12, TM15 and TM16, which are comprised of a catalytic domain with a proposed proton transport pathway; the outer wall constituted by the other 10 TMs traps the inner wall to sustain H^+-PPase function (Fig. 1b). Functional analyses authentically indicated that several residues in the inner wall are crucial for PP_i hydrolysis and proton translocation (Yang et al. 1999; Nakanishi et al. 2001; Van et al. 2005; Pan et al. 2011; Lin et al. 2012); however, detailed information on the structure/function relationship of the outer wall has yet to be validated.

Sequence alignment suggests that the amino acids in TM3 are highly conserved in plants (Fig. 1a). In addition, hydropathic analysis indicates that TM3 is relatively more hydrophilic than most other TMs in H^+-PPase (Fig. 1a, Supplementary Fig. S1). Moreover, the three-dimensional structure of *V. radiata* H^+-PPase (*Vr*H^+-PPase) reveals that TM5 and -6, which are the core TMs involved in H^+-PPase function, are near TM3 (Fig. 1b). It is thus proposed that TM3 interacts with TM5 and -6 to maintain the function of H^+-PPase. To verify this speculation, alanine-scanning mutagenesis was used in this study to investigate the role of TM3 in H^+-PPase. Each amino acid along TM3 was individually replaced with alanine, and the alanine residue was substituted by a serine. A set of site-specific constructs were generated and overexpressed in *Saccharomyces cerevisiae*; the microsomes extracted were used to determine their hydrolysis activities and proton translocation. The function of each residue in TM3 was then examined, and a working model was accordingly proposed to illustrate how TM3 maintains the structure and catalytic function of H^+-PPase.

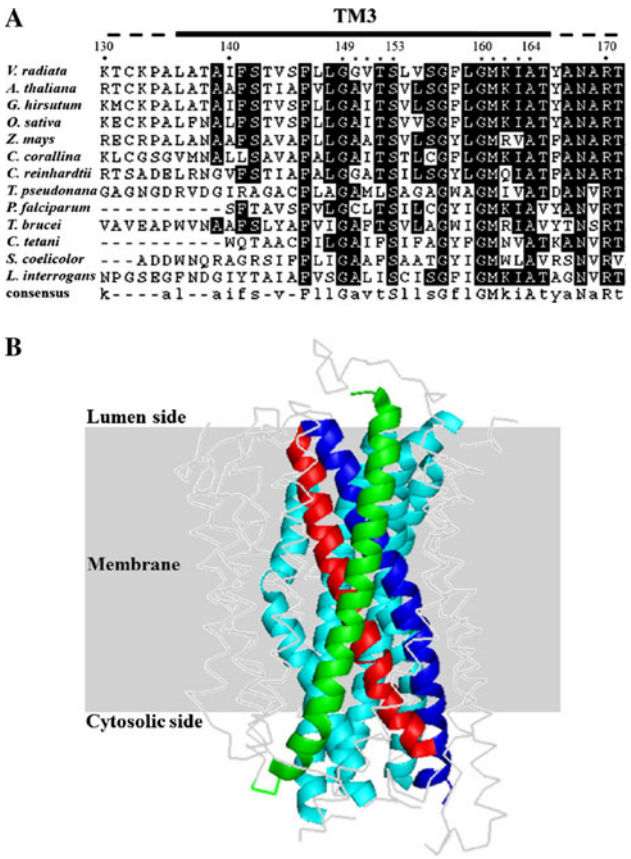

Fig. 1 The multiple sequence alignment of various H^+-PPases and X-ray crystal structure of *Vr*H^+-PPase. **a** The multiple sequence alignment was obtained using Biology Workbench 3.2 (Subramaniam 1998). The two GxxxG-like sequences are indicated with asterisks. The GenBank accession numbers for the H^+-PPase of each species are as follows: *Vigna radiata*, P21616; *Arabidopsis thaliana*, BAA32210; *Gossypium hirsutum*, ADN96173; *Oryza sativa*, BAA31523; *Zea mays*, NP_001106067; *Chara corallina*, BBA36841; *Chlamydomonas reinhardtii*, CAC44451; *Thalassiosira pseudonana*, XP_002289074; *Plasmodium falciparum*, AAD17215; *Trypanosoma brucei*, CBH10748; *Clostridium tetani*, NP_781083; *Streptomyces coelicolor*, Q9X913; and *Leptospira interrogans*, NP_711652. **b** X-ray crystal structure of *Vr*H^+-PPase. A ribbon representation of the monomeric structure of *Vr*H^+-PPase is depicted according to the crystal structure of *Vr*H^+-PPase (PDB 4A01) by PyMOL 1.5.0.4 (Schrodinger, New York, NY), containing 10 outer wall TMs (*gray* and *green*) and 6 inner core TMs (*cyan*, *blue* and *red*). TM3, TM5 and TM6 are marked in *green*, *blue* and *red*, respectively (Color figure online)

Materials and Methods

Mutagenesis and DNA Construction

The pBlueScript II SK(+) plasmid was used to clone and insert vacuolar H^+-PPase cDNA from *V. radiata* (GenBank™ accession number AB009077) between the *Hind*III and *Xba*I cut sites (Hung et al. 1995). Site-specific mutants within TM3 were constructed based on Megaprimer PCR (Barik 1997) and QuikChange PCR methods (Kirsch and Joly 1998). After the sequences were confirmed, the resulting mutated H^+-PPase cDNAs were cut and inserted into the *Escherichia coli*/*S. cerevisiae* shuttle vector pYES2 (Invitrogen, Carlsbad, CA) for yeast expression.

Expression in Yeasts and Preparation of Microsomes

The pYES2 vectors containing wild-type (WT) or mutated H^+-PPase cDNAs were transformed into a protease-deficient haploid strain of *S. cerevisiae*, BJ2168 (Kim et al. 1994; Pan et al. 2011) using the LiAc/polyethylene glycol method (Gietz et al. 1995). Transformed yeast cells were cultured as previously described (Hsiao et al. 2004). Microsomes from yeast cells were prepared using previous methods (Kim et al. 1995; Van et al. 2005).

Assay of Protein Concentration and Enzymatic Activities

Measurement of the microsomal protein concentration was based on the Bradford (1976) method using BSA as a standard. The production rate of P_i from PP_i represents the PP_i hydrolysis activity as previously described (Hsiao et al. 2007; Huang et al. 2010). Proton translocation was determined according to a previous protocol (Van et al. 2005; Pan et al. 2011). The background concentrations of K^+, Na^+ and Ca^{2+} in the assay buffer were below 4.0, 5.0 and 20 nM, respectively, as measured with an inductively coupled plasma-atomic emission spectrometer at the NTHU Instrument Center, National Tsing Hua University (Hsin Chu, Taiwan).

SDS-PAGE and Western Blotting Analysis

The procedure for SDS-PAGE was in accordance with the method of Laemmli (1970). The proteins in the gel were electrotransferred to a PVDF membrane, and the membrane was then incubated with antibodies using previously described methods (Van et al. 2005; Pan et al. 2011).

Trypsin Proteolysis

Microsomal proteins were digested with trypsin as described previously (Pan et al. 2011).

Results and Discussion

Expression and Enzymatic Activities of TM3 Mutants

Alanine-scanning mutagenesis was applied to explore the role of TM3 in *Vr*H^+-PPase. Each amino acid in TM3 was individually replaced with an alanine, and alanine residues were substituted with serine. The pYES2 vectors containing WT and mutated H^+-PPase genes were used to transform and expressed heterologously in the protease-deficient yeast strain BJ2168. Microsomes were extracted from yeast and utilized to determine the protein expression and enzymatic activity by Western blot and activity assays, respectively. The expression level of WT and mutant H^+-PPases was generally similar (Fig. 2a). The membrane fraction from the WT H^+-PPase displayed PP_i hydrolysis and PP_i-dependent H^+ transport activities of 23.3 ± 1.9 μmol PP_i (mg protein · h)$^{-1}$ and 17.5 ± 2.9 × 10^3 Δ*F* % (mg protein · h)$^{-1}$ (arbitrary units), respectively (Fig. 2b, c). Alanine/serine substitution at the G149, S153, G160, M161, I163 and A164 residues in the two putative helix–helix-interacting GxxxG-like motifs (Fig. 1a) (Schneider and Engelman 2004; Senes et al. 2004) and that at Y166 at

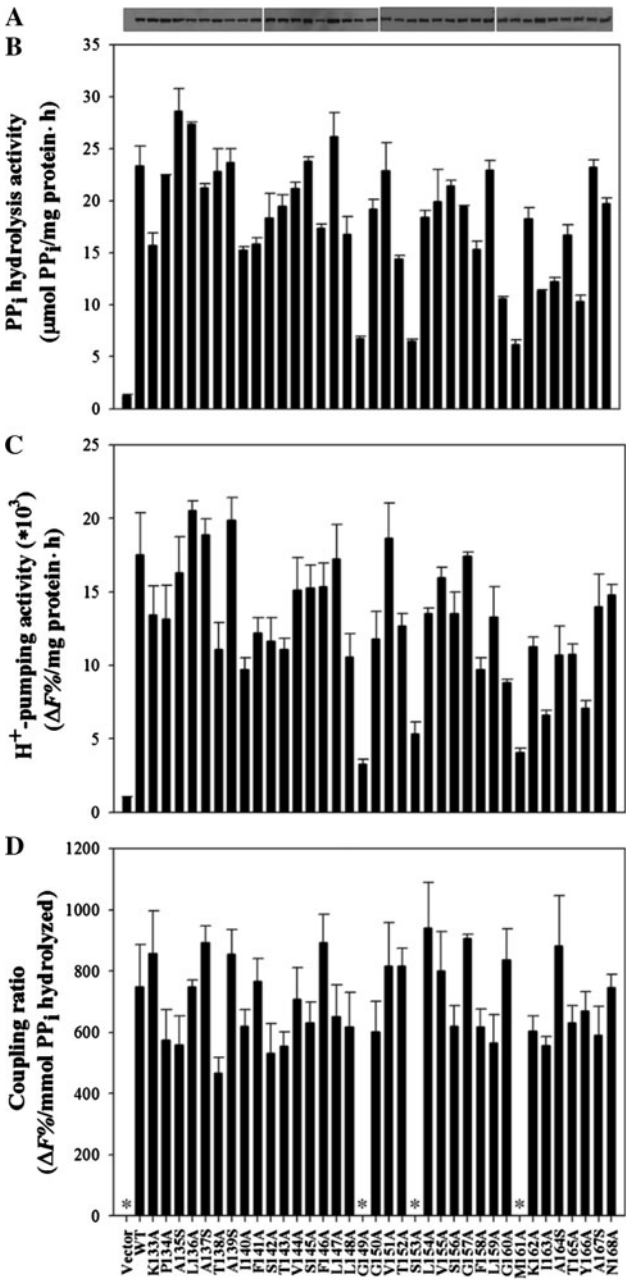

Fig. 2 Expression and enzymatic activities of H^+-PPase variants. **a** Expression level detected by Western blotting. **b** PP_i hydrolysis activities. **c** Proton translocation activities. **d** Coupling ratio. Thirty micrograms of microsomes from WT and H^+-PPase mutants were prepared for Western blotting. H^+-PPases were then recognized with an anti-H^+-PPase antibody. The PP_i hydrolysis and proton translocation activities for the WT were 23.3 ± 1.9 μmol PP_i (mg protein · h)$^{-1}$ and 17.5 ± 2.9 × 10^3 Δ*F* % (mg protein · h)$^{-1}$ (arbitrary units), respectively. The coupling ratio is the ratio of the initial proton pumping rate to PP_i hydrolysis, and that for WT was 7.5 ± 1.4 × 10^2 (Δ*F* % min^{-1}) (μmol PP_i hydrolyzed min^{-1})$^{-1}$, where Δ*F* % min^{-1} is the initial rate for the relative fluorescence quenching of acridine orange. The coupling ratios of the G149A, S153A and M161A mutants are difficult to calculate because of their poor enzymatic and proton translocation activities. Each value is expressed as the mean ± standard deviation from at least three independent experiments. *Asterisk* not determined

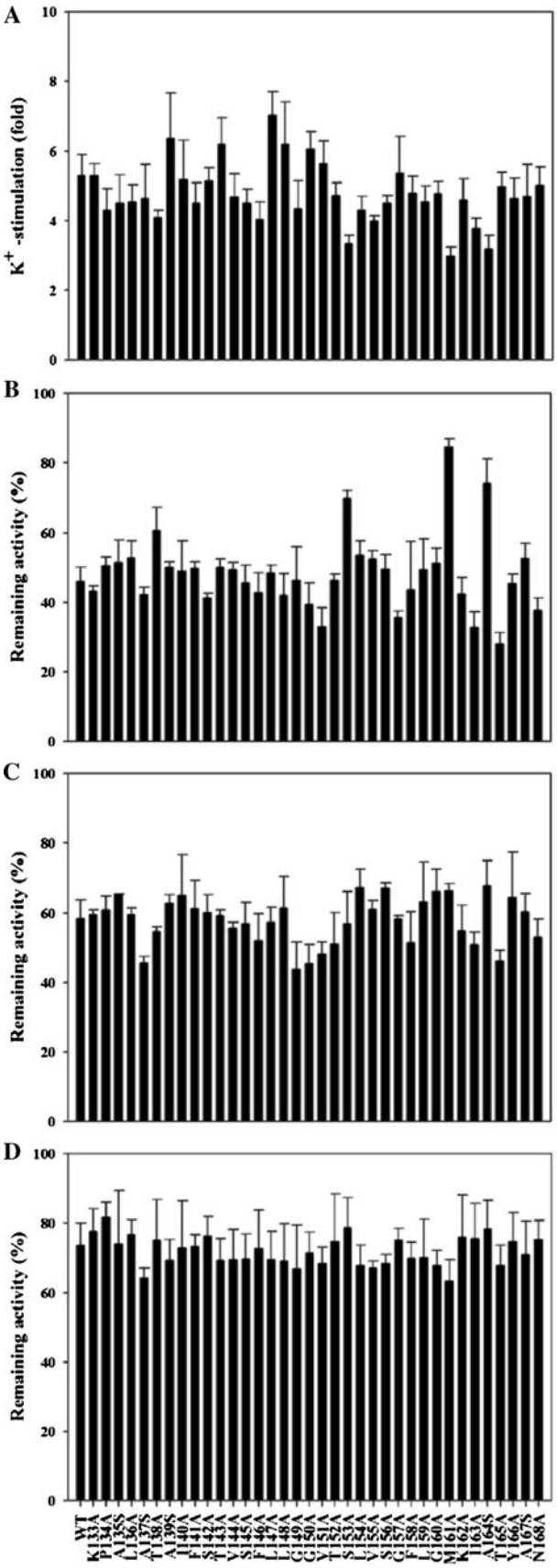

◀ **Fig. 3** Ion effects on H^+-PPase. **a** K^+, **b** Na^+, **c** Ca^{2+}, **d** F^-. The concentrations of K^+, Na^+, Ca^{2+} and F^- were 50 mM, 100 mM, 30 μM, and 10 mM, respectively. K^+ stimulation and Na^+, Ca^{2+} and F^- repression of enzymatic activity were obtained by calculating the ratio of hydrolysis activities in the presence and absence of the ions. Each value is expressed as the mean ± SD from at least three independent experiments

the membrane–cytosol interface resulted in relatively lower PP_i hydrolysis and proton translocation activities (Fig. 2b, c). It is conceivable that these residues are essential for the enzymatic activities of H^+-PPase. Furthermore, the K133A, I140A, F141A, L148A, T152A, F158A and T165A mutants exhibited 50–75 % of the PP_i hydrolytic and proton transport activities of WT (Fig. 2b, c), indicating that the bulky groups of these residues are involved in proper H^+-PPase function. The remaining variants displayed similar PP_i hydrolysis to WT, and most of these mutants showed comparable proton transport activities (Fig. 2b, c). However, several variants, such as the T138A, S142A, T143A, G150A and K162A mutants, maintained only 60–70 % of the proton transport activity of WT (Fig. 2c). Moreover, among all of the alanine/serine variants examined, the coupling ratios of the T138A and S142A mutants were decreased to approximately 60–70 % of that of WT, while those of the others were not noticeably different from WT (Fig. 2d). According to the *Vr*H^+-PPase crystallographic structure, the hydroxyl (OH) functional groups of T138 and S142, with one helix turn interval, face toward the inner wall, indicating that these residues might directly or indirectly participate in the proton translocation of H^+-PPase (Lin et al. 2012). Furthermore, some residues critical for PP_i hydrolysis, such as G149, I163 and Y166, could be involved in the maintenance of the heat tolerance of H^+-PPase (Supplementary Table S1). The T138A and G149A variants shifted the optimal pH toward the acidic or basic range, indicating the importance of T138 and G149 for H^+-PPase (Supplementary Table S1). Moreover, the Gaussian network model (Tirion 1996; Bakan et al. 2011; Lezon and Bahar 2012) suggests that TM3 displays higher dynamic cross-correlation to the putative proton transport residues (R242, D294, E301, K742) than other TMs of outer walls (Pan et al. 2011; Lin et al. 2012) (Supplementary Fig. S2). The essential residues in TM3 such as G149, S153, G160 and M161, which were shown to participate in enzymatic functions (Fig. 2), would probably be highly correlated with the putative proton transport residues for proton translocation of H^+-PPase (Supplementary Fig. S2). Taken together, all of the above-mentioned results unambiguously demonstrate that TM3 is responsible for the proper enzymatic and proton translocation activities of H^+-PPase, presumably through helix–helix interaction.

Ion Effects

To examine the effects of ions, the enzymatic activities of WT and mutant H^+-PPases were determined in the presence and absence of K^+, Na^+, Ca^{2+} and F^-. With 50 mM K^+, the PP_i hydrolytic activity of the WT was stimulated 5.3-fold (Fig. 3a). The further addition of 100 mM Na^+ inhibited enzymatic activity of the WT and most mutants by 45–60 % (Fig. 3b), suggesting that the Na^+ inhibition might interfere with K^+ binding. The K^+-mediated stimulation of the enzymatic activity of the S153A, M161A and A164S mutants was only 3-fold (Fig. 3a). In addition, these mutants displayed relatively lower susceptibility (20–40 %) to Na^+ inhibition than WT (55 %) (Fig. 3b). This determination suggested that the respective substitutions at S153, M161 and A164, leading to lower sensitivities to K^+ stimulation and Na^+ repression of PP_i hydrolysis, might result in structural deterioration at the K^+ (Na^+) binding site. The recent crystal structure of the *Vr*H^+-PPase showed that K^+ binds near the catalytic site of H^+-PPase to strengthen its catalytic structure and function (Maeshima 2000; Lin et al. 2012). The S153A, M161A and A164S variants exhibited lower PP_i hydrolysis activities (Fig. 2b), presumably resulting from their impairment in K^+ binding. These results definitively demonstrated that the S153, M161 and A164 residues in the TM3 of H^+-PPase are important for sustaining a proper conformation for K^+ binding and H^+-PPase functions. With the exception of the S153A, M161A and A164S mutants, the hydrolytic activity of the others was stimulated by K^+ similarly to that of WT (Fig. 3a). Nevertheless, the respective alanine substitutions for V151, G157, I163 and T165 led to an increase in the sensitivity to Na^+ inhibition (70 % inhibition) compared with WT (Fig. 3b). It is possible that Na^+ is prone to bind to these mutant H^+-PPases. In contrast, the susceptibility of the T138A mutant to Na^+ inhibition was reduced (40 % inhibition) (Fig. 3b).

In the presence of 30 μM Ca^{2+}, the hydrolysis of WT was suppressed to 60 % of its original values (Fig. 3c). The hydrolysis activities of the A137S, G149A, G150A and T165A variants were repressed even further, exhibiting only 45 % of their original activity levels, while Ca^{2+} inhibition on the hydrolysis of the other mutants was similar to that of WT. Ca^{2+} might suppress H^+-PPase by competing with Mg^{2+} to form Ca–PP_i (Maeshima 1991). It is thus speculated that A137, G149, G150 and T165 participate in maintaining the proper conformation for Mg^{2+} binding. Under treatment with 10 mM F^-, the inhibition of hydrolysis of all variants was similar to that of WT (30 % inhibition) (Fig. 3d), indicating that TM3 might not be involved in the inhibition of F^- in PP_i hydrolysis. Taking this into account, TM3 does not directly interact with PP_i even though it is crucial for the enzymatic activities of H^+-PPase.

Leucine Substitution at the Termini of GxxxG-Like Motifs

To further verify the function of the two putative helix–helix-interacting GxxxG-like motifs in TM3 of *Vr*H^+-PPase, the four residues (G149, S153, G160 and A164) at both termini of $G_{149}xxxS_{153}$ and $G_{160}xxxA_{164}$ were mutated to leucine with a bulky side chain (Fig. 4a, b), a strategy generally used for the detection of GxxxG-like motifs (cf., Polgar et al. 2004; Schneider and Engelman 2004; Faingold et al. 2012). With the exception of the G149L variant, all of the leucine mutants showed a similar expression level to that of WT (Fig. 4a). Subsequent observation of selection plates for the G149L mutant revealed a similar growth rate as WT (Fig. 4c), demonstrating that the cells contained the selection plasmid. Moreover, the selection plasmid in yeast was later shown to comprise the G149L H^+-PPase gene (data not shown). It is conceivable that the G149L mutant protein either is lost before trafficking to microsomal membranes or fails to insert into microsomal membranes (Pan et al. 2011). To explore the distribution of the G149L mutant protein in yeast cells, Western blotting analysis was subsequently used to identify the protein expression in cytosolic and membrane fractions (Fig. 4d). WT *Vr*H^+-PPase was detected in the membrane fraction, while the G149L variant was observed neither in the membrane nor in the cytosolic fractions, suggesting that the failure of protein trafficking was not responsible for the improper expression of the G149L mutant. Instead, the G149L mutant, which was not expressed in the membrane, might be rapidly turned over, presumably due to its unfolded conformation (see Duan et al. 2011). It is thus inferred that the stability of the regions around G149 is essential for the efficient expression of H^+-PPase. The variants with a bulky leucine residue, i.e., the G149L, S153L, G160L and A164L mutants, expressed lower enzymatic activities and proton translocation than their corresponding alanine variants, i.e., the G149A, S153A, G160A and A164S mutants, and WT (Figs. 2b, c, 4b). Their coupling ratios were thus difficult to determine because of poor enzymatic activities, and those for the G149A and S153A mutants were also hard to calculate (Fig. 4b). Nevertheless, the G160A and A164S mutants exhibited similar coupling ratios to WT. It has been shown that the GxxxG motif (interval of any three residues between the two glycine residues) and the GxxxG-like motif (one or both glycine residues are replaced by other small residues, such as alanine or serine) in TMs often maintain the associations between TMs through interhelical van der Waals contacts (MacKenzie et al. 1997; Russ and Engelman 2000; Schneider and Engelman 2004; Senes et al. 2004). The interactions coming from the proximity between TMs are presumably promoted by the

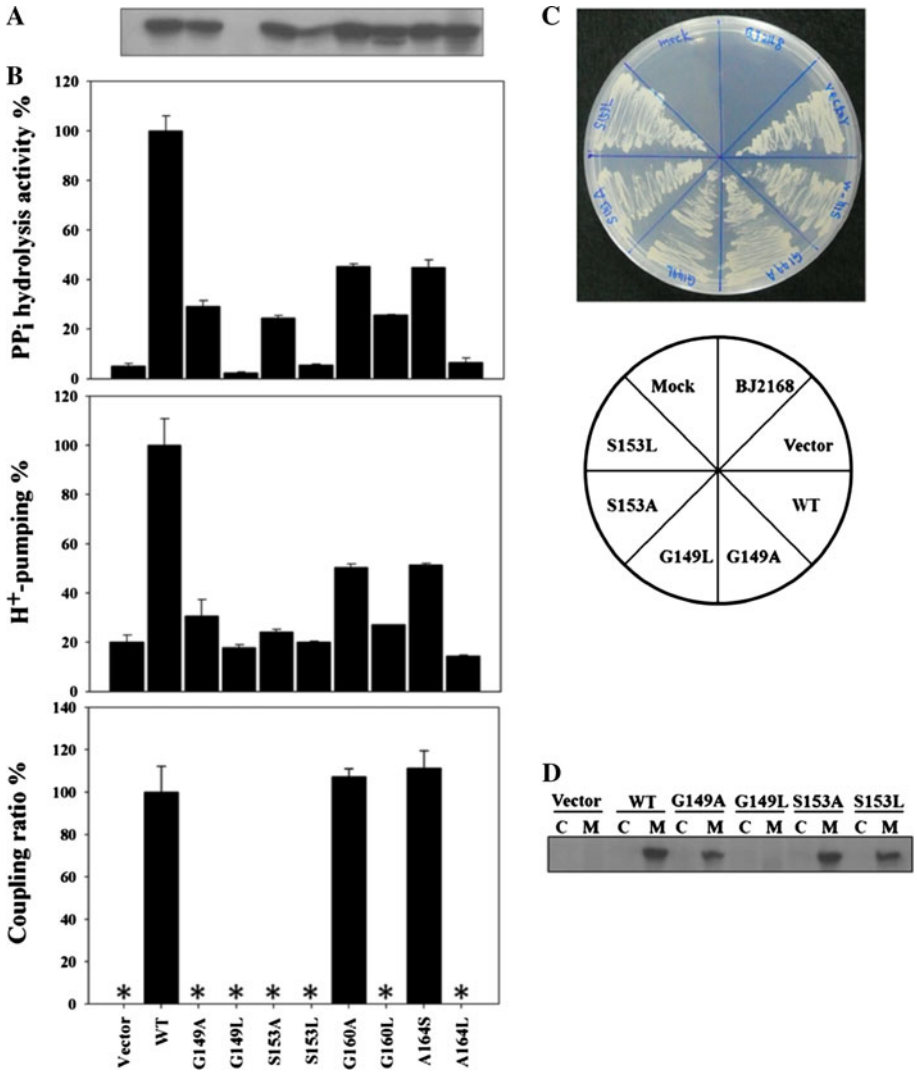

Fig. 4 Expression and activities of alanine- and leucine-substituted variants mutated at the termini of the GxxxG-like motifs. **a** Expression level detected by Western blotting. **b** Enzymatic activities. **c** Growth of BJ2168 yeast cells harboring expression vectors in the selection plate. **d** Identification of H^+-PPases in soluble or membrane fractions. Expression and enzymatic activities of H^+-PPases were determined as in Fig. 2. Each value is expressed as the mean ± SD from at least three independent experiments. *Asterisk* not determined. Sixty micrograms of proteins from membrane (*M*) and cytoplasmic (*C*) fractions were prepared for Western blotting and recognized with anti-His antibody

small residues at the termini of the two motifs. Moreover, the side chains of the terminal residues would possibly participate in the maintenance of associations between TMs. The above results demonstrated that the leucine mutants showed lower enzymatic activities than the alanine mutants, implying that the bulky side chain led to an increase of distances between TM3 and other TMs more than did small side chains of alanine or serine, which lessen the interactions (Fig. 4b). Besides, the destruction of original hydrogen bonding of S153 by leucine substitution likely resulted in weaker interactions between TM3 and other TMs and consequently the loss of enzymatic function in H^+-PPase (Dawson et al. 2002; Schneider and Engelman 2004). Hence, these four small amino acids (G149, S153, G160 and A164) at the termini of the $G_{149}xxxS_{153}$ and $G_{160}xxxA_{164}$ motifs in TM3 are necessary for the conformational stability and enzymatic activities of H^+-PPase, which is consistent with the characteristics of the GxxxG-like motif (cf., Curran and Engelman 2003; Schneider and Engelman 2004; Lo et al. 2011; Faingold et al. 2012) (Supplementary Table S2). Moreover, functional analyses and X-ray crystal structure confirmed the importance of these four small residues in the interaction of TM3 with other TMs (Supplementary Table S3; Fig. S3). It has been shown that phenylalanine could enhance the interaction between TMs through GxxxG, GxxxS and GxxxA motifs (Unterreitmeier et al. 2007). Likewise, the experimental results in this study revealed that F146 with two residues upstream of the N terminus of $G_{149}xxxS_{153}$ is crucial for thermal stability of H^+-PPase (Supplementary Table S1), implying that F146 conceivably stabilizes $G_{149}xxxS_{153}$ motif and maintains proper heat tolerance of H^+-PPase (Supplementary Table S1; Fig. S3). In short, these results confirmed that the two motifs in TM3 act as GxxxG-like motifs, and their terminal residues are indispensable for H^+-PPase.

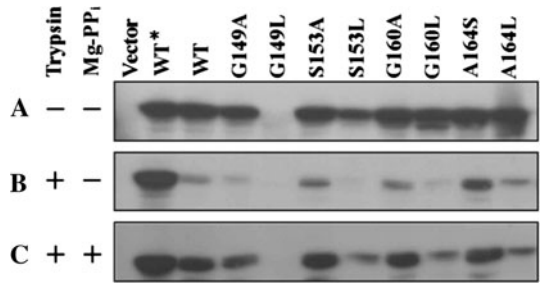

Fig. 5 Trypsinolysis of alanine- and leucine-substituted mutants at the termini of the GxxxG-like motifs. **a** Control without trypsin treatment. **b** Treatment with trypsin. **c** Treatment with trypsin in the presence of Mg–PP_i. The procedure of trypsinolysis was based on a previous study (Pan et al. 2011). *Asterisk* control without any treatment

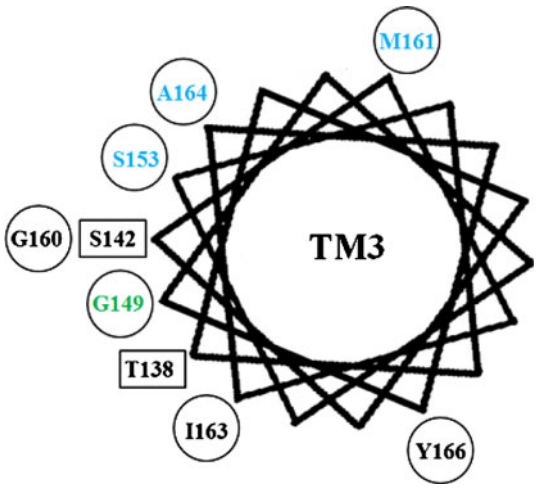

Fig. 6 Helix wheel of TM3 showing residues related to the enzymatic activities and proton transport of H^+-PPase. Amino acids that are important for the enzymatic function of H^+-PPase are circled. Residues that are associated with the efficient proton transport of H^+-PPase are enclosed by rectangles. The S153, M161 and A164 (*blue*) residues are critical for the K^+-mediated stimulation of H^+-PPase. The G149 (*green*) residue is involved in optimal reaction pH and thermal stability of H^+-PPase. The stability of the area surrounding G149 is also necessary for the proper expression of H^+-PPase (Color figure online)

Trypsinolysis

Trypsinolysis was used to demonstrate the conformational changes of the alanine/serine and leucine-substituted mutants at the termini of the two GxxxG-like motifs in TM3 (Fig. 5). The WT H^+-PPase underwent considerable proteolysis by trypsin (Fig. 5b). However, addition of the physiological substrate Mg–PP_i provided relative protection against trypsin digestion (Fig. 5c) (Pan et al. 2011). With the exception of the G149A variant, the alanine/serine mutants were relatively resistant to trypsin digestion compared with WT in the absence of Mg–PP_i. Nevertheless, the leucine mutants were more vulnerable to trypsin digestion. In addition, the WT and most of the alanine/serine mutants, with the exception of G149A variant, displayed similar substrate protection against trypsin in the presence of Mg–PP_i. However, substrate protection for the leucine mutants was rather low compared with WT. The above results showed that leucine-substituted mutants were more susceptible to trypsin digestion than the WT and alanine-substituted proteins (Fig. 5b, c). It is thus speculated that the bulky leucine moiety at either terminus of the two GxxxG-like motifs destabilized the protein configuration, promoting trypsin attack at K250, the first digestion site in H^+-PPase (Lee et al. 2011; Lin et al. 2012). Furthermore, the necessity of the terminal residues for the proper conformation of the H^+-PPase is also indicated, which is consistent with the properties of GxxxG-like motifs.

The residues that are critical for the function of H^+-PPase in TM3 are depicted in Fig. 6. Most of these amino acids are located at the left side of the helix wheel shown. It is indicated that T138 and S142, whose side chains face toward the core TMs, are involved in the efficient proton transport of H^+-PPase. Two GxxxG-like motifs in TM3 were revealed to be crucial for the enzymatic activities and structural stability of H^+-PPase. Furthermore, the stability of the area surrounding G149 is critical for the proper expression of H^+-PPase. S153, M161 and A164 are pivotal for the K^+-mediated stimulation of H^+-PPase. Taken together, this study demonstrates that TM3 plays essential functional/structural roles in H^+-PPase.

Acknowledgments We thank Meng-Je Juang and Tien-Yang Ma for their technical assistance with DNA construction. This study was supported by Grants from the National Science Council, Taiwan (NSC 100-2311-B-007-001-MY3, NSC 101-2627-M-007-008 and NSC 101-2120-M-007-001).

References

Bakan A, Meireles LM, Bahar I (2011) ProDy: protein dynamics inferred from theory and experiments. Bioinformatics 27:1575–1577

Barik S (1997) Mutagenesis and gene fusion by megaprimer PCR. In: White BA (ed) PCR cloning protocols: from molecular cloning to genetic engineering. Humana Press, Totowa, pp 173–182

Bradford MM (1976) A rapid and sensitive method for the quantitation of microgram quantities of protein utilizing the principle of protein dye binding. Anal Biochem 72:248–254

Curran AR, Engelman DM (2003) Sequence motifs, polar interactions and conformational changes in helical membrane proteins. Curr Opin Struct Biol 13:412–417

Dawson JP, Weinger JS, Engelman DM (2002) Motifs of serine and threonine can drive association of transmembrane helices. J Mol Biol 316:799–805

Drozdowicz YM, Rea PA (2001) Vacuolar H^+-pyrophosphatases: from the evolutionary backwaters into the mainstream. Trends Plant Sci 6:206–211

Drozdowicz YM, Kissinger JC, Rea PA (2000) AVP2, a sequence-divergent, K^+-insensitive H^+-translocating inorganic pyrophosphatase from *Arabidopsis*. Plant Physiol 123:353–362

Duan P, Wu J, You G (2011) Mutational analysis of the role of GXXXG motif in the function of human organic anion transporter 1 (hOAT1). Int J Biochem Mol Biol 2:1–7

Faingold O, Cohen T, Shai Y (2012) A GxxxG-like motif within HIV-1 fusion peptide is critical to its immunosuppressant activity, structure, and interaction with the transmembrane domain of the T-cell receptor. J Biol Chem 287:33503–33511

Gietz RD, Schiestl RH, Willems AR, Woods RA (1995) Studies on the transformation of intact yeast cells by the LiAc/SS-DNA/PEG procedure. Yeast 11:355–360

Gordon-Weeks R, Steele SH, Leigh RA (1996) The role of magnesium, pyrophosphate, and their complexes as substrates and activators of the vacuolar H^+-pumping inorganic pyrophosphatase (studies using ligand protection from covalent inhibitors). Plant Physiol 111:195–202

Hsiao YY, Van RC, Hung SH, Lin HH, Pan RL (2004) Roles of histidine residues in plant vacuolar H^+-pyrophosphatase. Biochim Biophys Acta 1608:190–199

Hsiao YY, Pan YJ, Hsu SH, Huang YT, Liu TH, Lee CH, Lee CH, Liu PF, Chang WC, Wang YK, Chien LF, Pan RL (2007) Functional roles of arginine residues in mung bean vacuolar H^+-pyrophosphatase. Biochim Biophys Acta 1767:965–973

Huang YT, Liu TH, Chen YW, Lee CH, Chen HH, Huang TW, Hsu SH, Lin SM, Pan YJ, Lee CH, Hsu IC, Tseng FG, Fu CC, Pan RL (2010) Distance variations between active sites of H^+-pyrophosphatase determined by fluorescence resonance energy transfer. J Biol Chem 285:23655–23664

Hung SH, Chiu SJ, Lin LY, Pan RL (1995) Vacuolar H^+-pyrophosphatase cDNA (accession no. U31467) (PGR 95-082) from etiolated mung bean seedlings. Plant Physiol 109:1125–1127

Kim EJ, Zhen RG, Rea PA (1994) Heterologous expression of plant vacuolar pyrophosphatase in yeast demonstrates sufficiency of the substrate-binding subunit for proton transport. Proc Natl Acad Sci USA 91:6128–6132

Kim EJ, Zhen RG, Rea PA (1995) Site-directed mutagenesis of vacuolar H^+-pyrophosphatase: necessity of Cys634 for inhibition by maleimides but not catalysis. J Biol Chem 270:2630–2635

Kirsch RD, Joly E (1998) An improved PCR-mutagenesis strategy for two-site mutagenesis or sequence swapping between related genes. Nucleic Acids Res 26:1848–1850

Laemmli UK (1970) Cleavage of structure proteins during the assembly of the head of bacteriophage T4. Nature 222:680–685

Lee CH, Pan YJ, Huang YT, Liu TH, Hsu SH, Lee CH, Chen YW, Lin SM, Huang LK, Pan RL (2011) Identification of essential lysines involved in substrate binding of vacuolar H^+-pyrophosphatase. J Biol Chem 286:11970–11976

Lezon TR, Bahar I (2012) Constraints imposed by the membrane selectively guide the alternating access dynamics of the glutamate transporter GltPh. Biophys J 102:1331–1340

Lin SM, Tsai JY, Hsiao CD, Huang YT, Chiu CL, Liu MH, Tung JY, Liu TH, Pan RL, Sun YJ (2012) Crystal structure of a membrane-embedded H^+-translocating pyrophosphatase. Nature 484:399–403

Liu TH, Hsu SH, Huang YT, Lin SM, Huang TW, Chuang TH, Fan SK, Fu CC, Tseng FG, Pan RL (2009) The proximity between C-termini of dimeric vacuolar H^+-pyrophosphatase determined using atomic force microscopy and a gold nanoparticle technique. FEBS J 276:4381–4394

Lo A, Cheng CW, Chiu YY, Sung TY, Hsu WL (2011) TMPad: an integrated structural database for helix-packing folds in transmembrane proteins. Nucleic Acids Res 39:D347–D355

MacKenzie KR, Prestegard JH, Engelman DM (1997) A transmembrane helix dimer: structure and implications. Science 276:131–133

Maeshima M (1991) H^+-translocating inorganic pyrophosphatase of plant vacuoles: inhibition by Ca^{2+}, stabilization by Mg^{2+} and immunological comparison with other inorganic pyrophosphatases. Eur J Biochem 196:11–17

Maeshima M (2000) Vacuolar H^+-pyrophosphatase. Biochim Biophys Acta 1465:37–51

Maeshima M (2001) Tonoplast transporters: organization and function. Annu Rev Plant Physiol Plant Mol Biol 52:469–497

Nakanishi Y, Saijo T, Wada Y, Maeshima M (2001) Mutagenic analysis of functional residues in putative substrate-binding site and acidic domains of vacuolar H^+-pyrophosphatase. J Biol Chem 276:7654–7660

Pan YJ, Lee CH, Hsu SH, Huang YT, Lee CH, Liu TH, Chen YW, Lin SM, Pan RL (2011) The transmembrane domain 6 of vacuolar H^+-pyrophosphatase mediates protein targeting and proton transport. Biochim Biophys Acta 1807:59–67

Polgar O, Robey RW, Morisaki K, Dean M, Michejda C, Sauna ZE, Ambudkar SV, Tarasova N, Bates SE (2004) Mutational analysis of ABCG2: role of the GXXXG motif. Biochemistry 43:9448–9456

Russ WP, Engelman DM (2000) The GxxxG motif: a framework for transmembrane helix–helix association. J Mol Biol 296:911–919

Schneider D, Engelman DM (2004) Involvement of transmembrane domain interactions in signal transduction by α/β integrins. J Biol Chem 279:9840–9846

Senes A, Engel DE, DeGrado WF (2004) Folding of helical membrane proteins: the role of polar, GxxxG-like and proline motifs. Curr Opin Struct Biol 14:465–479

Serrano A, Perez-Castineira JR, Baltscheffsky H, Baltscheffsky M (2004) Proton-pumping inorganic pyrophosphatases in some Archaea and other extremophilic prokaryotes. J Bioenerg Biomembr 36:127–133

Subramaniam S (1998) The biology workbench—a seamless database and analysis environment for the biologist. Proteins 32:1–2

Tirion MM (1996) Large amplitude elastic motions in proteins from a single parameter, atomic analyses. Phys Rev Lett 77:1905–1908

Unterreitmeier S, Fuchs A, Schaffler T, Heym RG, Frishman D, Langosch D (2007) Phenylalanine promotes interaction of transmembrane domains via GxxxG motifs. J Mol Biol 374:705–718

Van RC, Pan YJ, Hsu SH, Huang YT, Hsiao YY, Pan RL (2005) Role of transmembrane segment 5 of the plant vacuolar H^+-pyrophosphatase. Biochim Biophys Acta 1709:84–94

Yang SJ, Jiang SS, Kuo SY, Hung SH, Tam MF, Pan RL (1999) Localization of carboxylic residues possible involved in the inhibition of vacuolar H^+-pyrophosphatase by *N*,*N*′-dicyclohexylcarbodiimide. Biochem J 342:641–646